

## **Pitting Corrosion Evaluation of Titanium in NaBr Solutions by Electrochemical Methods and Raman Spectroscopy**

Rinat Ittah<sup>1,\*</sup>, Itamar Malka<sup>2</sup>, Ilana Bar<sup>2</sup> and David Itzhak<sup>1</sup>

<sup>1</sup> Department of Materials Engineering, Ben-Gurion University of the Negev, Beer-Sheva 84105, Israel.

<sup>2</sup> Department of Physics, Ben-Gurion University of the Negev, Beer-Sheva 84105, Israel.

\*E-mail: [Ittahr@bgu.ac.il](mailto:Ittahr@bgu.ac.il)

*Received: 27 October 2014 / Accepted: 8 December 2014 / Published: 16 December 2014*

---

The behavior of passive titanium grade 2 (Ti-2) alloy in sodium bromide solutions of different concentrations, following induction of an electric field, was characterized by cyclic potentiodynamic polarization and electrochemical impedance spectroscopy. The outcome of this exposure was assessed by morphologic characterization via scanning electron microscopy and by depth layer element analysis with X-ray photoelectron spectroscopy. In relatively diluted solutions, the Ti-2 had shown sensitivity to pitting corrosion and breakdown of the passivation layer, while in saturated solution no pitting was encountered, indicating an anomalous behavior for the latter. This was confirmed by measurement of the Raman spectra of the different solutions, which showed that the amount of free water molecules is negligible in saturated solutions and in fact the ultimate majority of water molecules are bounded to the dissolved ions. The implications of these factors on Ti-2 corrosion will be discussed.

---

**Keywords:** Titanium, pitting, sodium bromide, saturation, electrochemical impedance spectroscopy, polarization, Raman spectroscopy

### **1. INTRODUCTION**

Titanium and titanium-alloys are attractive metallic materials widely used in medicine, dentistry and aeronautical applications [1-3]. This is partly due to their excellent corrosion resistance in many aqueous environments, provided by spontaneous formation of a passive titanium dioxide (TiO<sub>2</sub>) film, which is approximately 1 nm thick. Ti shows marked resistance to uniform corrosion in seawater, wet chloride media and diluted or concentrated chloride or bromide environments [4]. Lesser resistance can be observed in hydrofluoric acid solution because fluoride ions form highly stable and

soluble complexes with  $Ti^{+3}$ , which lead to aggressive attack of Ti alloys over a full range of concentrations.

Actually, pitting corrosion can be observed on Ti surfaces under anodic polarization in bromide containing aqueous solutions, mainly in HBr media [5]. This behavior is attributed to a significant decrease in the anodic breakdown potential under bromide environments [6,7]. Hou and Meng suggested that pit initiation of pure titanium in bromide solutions is related to the absorption of  $Br^-$  at the oxide/solution interface and formation of bromide nuclei such as  $TiBr$  [8]. Furthermore, it was suggested [8] that  $TiO_2$  repassivates the surface and therefore decreases the dissolution at the micro-pits, as long as  $Br^-$  concentration is low ( $\leq 0.5$  M). However, at higher  $Br^-$  ion concentrations ( $> 0.5$  M), local aggressive conditions are established and an increase in the mass transfer occurs, leading to a decrease in the passive film resistance [9]. Blasco *et al.* [10] investigated the behavior of titanium in concentrated LiBr solution that is used in absorbing air conditioning machines and found that the pitting corrosion susceptibility of titanium increased with LiBr concentration. Moreover, in our previous study [11] it was reported that titanium in ammonium bromide solutions had shown anomalous behavior in pitting sensitivity. Particularly, under saturation conditions, positive hysteresis loop was not recorded under anodic polarization and electrochemical impedance spectroscopy (EIS) showed an increase in resistance with time without an inductive element in the equivalent electrical circuits.

Furthermore, attention has been given to the effects of ions on water structure [12-14]. It was found that small highly charged ions, such as  $F^-$  and  $Na^+$ , bind stronger to a water molecule than one water molecule to another [14]; these ions can be classified as “structure maker” or kosmotropes. On the other hand, large monovalent ions such as  $I^-$ ,  $Br^-$  and  $Cl^-$  exhibit weaker interactions to a neighborhood water molecule than a water molecule to another water molecule, therefore are assigned as “structure breaker” or chaotropes.

One of the valuable methods that has been proven in studying water structure is Raman spectroscopy [15], which is one of the vibrational spectroscopies. For example, Li *et al.* [16] analyzed the Raman spectra of the O-H stretching band of sodium halide solutions at concentrations of 0-1 M, using deconvolution of five Gaussian components with center frequencies of 3051, 3233, 3393, 3511 and 3628  $cm^{-1}$ , where each of them indicates particular configuration of the water structure. They found that the increase of the concentration of large ions would encourage decrease in free water molecules or free O-H. On the other hand, water molecules with nearby small ions such as  $F^-$  tend to form hydrogen bond with the ion, therefore the amount of free water molecules or free O-H increases with ion concentration. Free water molecule is a molecule with no any type of bonds with a neighbor molecule [14].

The present study focuses on the electrochemical behavior of titanium in a full range of concentrations of sodium bromide (NaBr) from 0.01 M to the saturated solution (about 7 M) at ambient conditions. The purpose of this work is to examine by different characterization methods the behavior of titanium grade 2 (Ti-2) alloy under sodium bromide solutions. This will allow to compare the behavior with that found in ammonium bromide solutions [11] and to find out whether similar behavior is encountered for Ti-2 under saturation.

Here we will evaluate the pitting sensitivity of Ti-2 in NaBr aqueous solutions using the EIS technique, cyclic polarization measurements and scanning electron microscopy (SEM) and X-ray

photoelectron spectroscopy (XPS) observations. In addition, the anomalous behavior of such media under saturated condition had been studied by Raman spectroscopy. This technique showed change in the O-H bonds of H<sub>2</sub>O molecules with increasing the concentration of brine solutions; which further modifies the chemical activity of the concentrated solutions and may lead to unexpected results.

## 2. MATERIALS AND METHODS

The tests were performed in three electrodes cylindrical cell using platinum as a counter electrode and standard Ag/AgCl (3.5 M KCl) as a reference electrode [11]. The working electrodes were made from unalloyed Ti-2 with maximum content of: 0.3 Fe wt.%, 0.1 C wt.%, 0.25 O wt.% and 0.03 N wt.% . The area of the working electrode was 4.5 cm<sup>2</sup>. The working electrode samples were cut from a 2 mm width plate. Prior to exposure, the tested coupons that acted as working electrodes were polished with SiC paper to 500 grit, rinsed with de-ionized water and dried with acetone. We designed the electrochemical cell, to stimulate the pitting attack combined with crevice developed under the Teflon gasket. The apparatus exposes large area of the working electrode located parallel to the counter electrode, where both of them have the same size. In this cell the electrical field is homogeneous and the direction of the electrical field is perpendicular to the surface exposed to the environment under the anodic conditions.

Test solutions containing NaBr at concentrations of 0.01, 0.1, 1 and 7 M were used. The aqueous solutions were prepared from commercial solid NaBr and de-ionized water (resistivity of 18 mΩ cm).

Polarization and alternating current (AC) impedance measurements were carried out on Versa stat 3, a computer controlled potentiostat system, using the V3 studio software. Cyclic potentiodynamic polarization curves were made using a scan rate of 1 mV/s. Electrochemical impedance spectra were made using frequencies in the 1000 - 0.01Hz range with 100 μA root mean square (RMS) amplitude using potentiostatic technique at ambient conditions. The EIS were made on titanium plates exposed in one run and then inspected by SEM model JEOL J38-35CF. Four samples were used in each solution under the following anodic potential: passivity at 0.3 V vs. Ag/AgCl and over the break down potential at 1.6 and 2 V vs. Ag/AgCl. EC-Lab® V10.0 software was used to adapt equivalent circuits to the experiments.

XPS data were collected using an ultrahigh vacuum ( $1 \times 10^{-9}$  bar) X-ray photoelectron spectrometer (Thermo Scientific ESCALAB 250) with an Al K $\alpha$  X-ray source and a monochromator. The X-ray beam size was 500 μm and survey spectra was recorded with pass energy (PE) 150 eV and high energy resolution spectra were recorded with PE of 20 eV. To correct for charging effects, all spectra were calibrated relative to a carbon 1s peak positioned at 285.0 eV. The depth profile of the sample was obtained by combining a sequence of Ar ion gun etch cycles interleaved with XPS measurements from the current surface. The sputtering rate was of about 0.07 nm/s. Processing of the XPS results was carried out using the AVANTGE program.

Raman spectra of the NaBr solutions were measured by a home built Raman spectrometer. The beam delivered by a Q-switched microchip laser (Horus Laser, HLW-G-F010-11101), operating

at 532 nm at a repetition rate of 10.6 kHz with pulses of  $\sim 900$  ps duration (full-width-half maximum) and power of about 200 mW, was used for excitation. The laser beam was turned by a dichroic mirror and a  $90^\circ$  tiny prism (3 mm) and was tightly focused through x 40/0.65 microscope onto the particular samples, hold in a 1 cm diameter glass vials. The backscattered Raman signal was collimated by the same objective and filtered by a long-wavepass edge filter (Semrock, LP03-532RE-25). This signal was focused with a  $\sim f/4$  lens, onto a pinhole (100  $\mu\text{m}$ ) located in front of a slit of a 0.14 m spectrometer (Jobin–Yvon, MicroHR) to match its f/3.88 entrance aperture ratio. The spectrometer was equipped with a 1,200-lines/mm grating and eventually an air cooled 1,024 x 1,024 intensified charged coupled device (ICCD) (Andor, DH734-18U), driven by the Solis 4.15 software, for signal collection. The Raman spectra of the OH stretching region of water were recorded in the region between 2500 and 4000  $\text{cm}^{-1}$ , while operating the ICCD for integration times of 1 s with ten accumulations. All the spectra were measured at ambient temperature.

### 3. RESULTS AND DISCUSSION

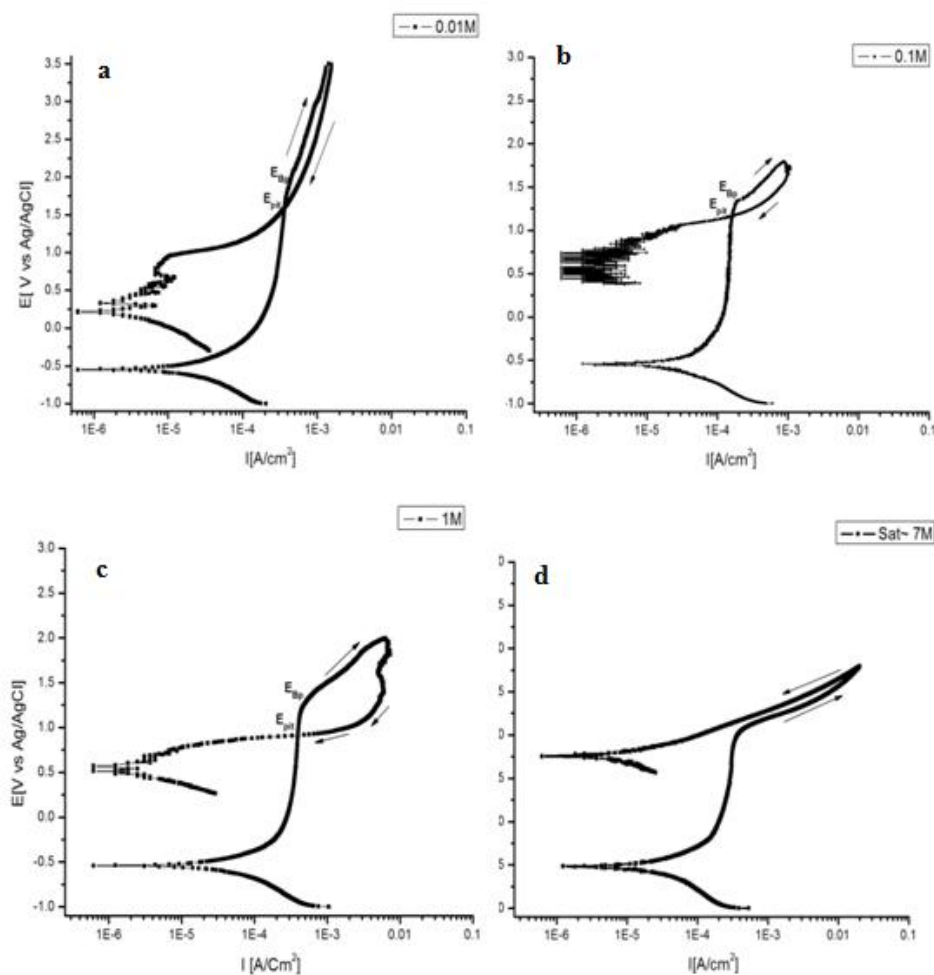


**Figure 1.** Cyclic potentiodynamic polarization curves for NaBr solutions: (a) 0.01 M, (b) 0.1 M, (c) 1 M and (d) saturate solution.

**Table 1.** Electrochemical corrosion parameters of Ti grade 2 as a function of NaBr concentration at ambient temperature

[NaBr]	$E_{corr}$	$i_{corr}$	$E_{BP}$	$E_{pit}$
M	[V] vs Ag/AgCl	A/cm <sup>2</sup>	[V] vs Ag/AgCl	[V] vs Ag/AgCl
0.01	-0.55	$1.8 \times 10^{-5}$	1840	1600
0.1	-0.56	$3.1 \times 10^{-5}$	1350	1240
1.0	-0.56	$6.8 \times 10^{-5}$	1270	900
Saturation	-0.51	$3.4 \times 10^{-5}$	--	--

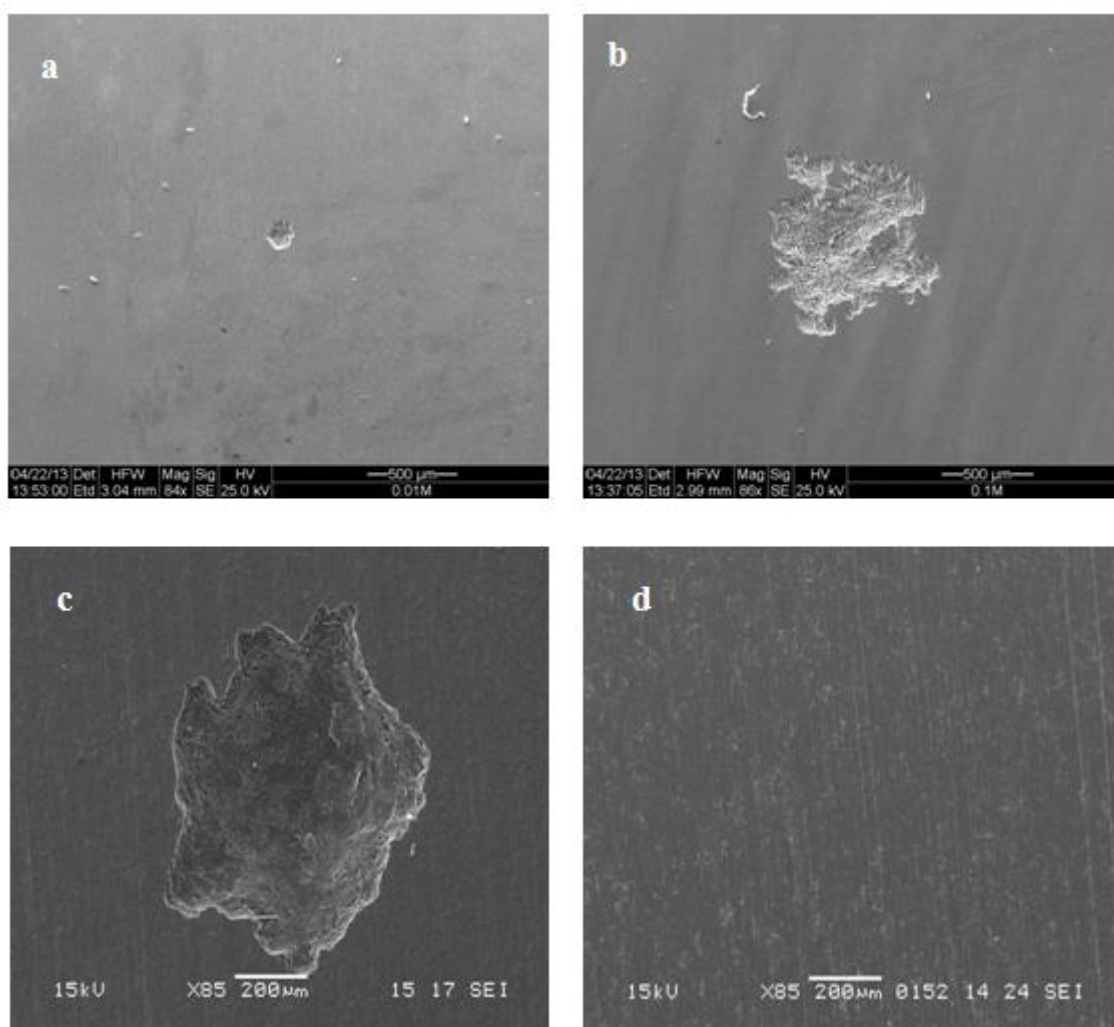


**Figure 2.** SEM observations for Ti-2 in NaBr solutions of different concentrations: (a) reference sample, (b) 1 M, (c) 4 M and (d) saturated.

Cyclic potentiodynamic polarization curves of a Ti-2 coupon exposed to NaBr solutions of different concentrations, at ambient temperature, are shown in Fig. 1(a-d). The average corrosion potentials estimated from these curves, pitting potential ( $E_{pit}$ ), breakdown potential ( $E_{BP}$ ) and the corrosion current densities ( $I_{corr}$ ) that were obtained from the polarization curves by Tafel

extrapolations are summarized in Table 1. No significant changes in corrosion potential were observed, however, according to the corrosion current density values, increasing the concentration of bromide up to 1 M has driven uniform corrosion attack of Ti-2 in NaBr environment. Increasing the concentration up to saturation, results in decrease of the corrosion rates. The meaning of such behavior is a decrease in the chemical activity of the salty solutions under saturation.

Furthermore, the cyclic polarization curve for the Ti-2 in NaBr solution of 0.01 M, indicates rapid increase in corrosion current density with the increase of anodic potential due to metal anodic dissolution. At a certain stage with the rise of anodic potential in the positive direction, passivity appears with no significant change in current density until the breakdown potential is reached, at approximately 2 V vs. the Ag/AgCl reference electrode. This finding points to formation of a protective passive film that acts as a diffusion barrier between the metal surface and the electrolyte. Upon reversing the potential sweep, from anodic to cathodic direction, the pitting potential is observed at lower value than the breakdown potential, meaning emergence of a positive hysteresis loop. The appearance of a positive hysteresis loop in cyclic potentiodynamic polarization test indicates a delay in repassivation of an existing pit that continues to dissolve. According to [17-18], larger hysteresis loop indicates higher sensitivity to pitting. Hence, it can be seen that the discussed system (0.01 M) shows a minor sensitivity to local corrosion.

According to the cyclic potentiodynamic polarization curves, the increase of the NaBr concentration to 0.1 M is characterized by similar behavior, however, it is noted that both  $E_{\text{pit}}$  and  $E_{\text{BP}}$  shift to lower potential and the hysteresis loop gets wider. This behavior is more significant in presence of 1 M NaBr solution. These findings reveal that increase in bromide concentration has a significant effect on the tendency of titanium to localized corrosion attack in NaBr environment. Moreover, during depolarization of 0.1 and 1 M concentrations cyclic current oscillations were observed near 1.8 V vs. Ag/AgCl. These oscillations indicate instability in the electrical resistivity of the surface.

The cyclic potentiodynamic polarization curve of titanium in saturated NaBr solution indicates also an active-passive transition and a sharp increase in current density at anodic potential of 1.06 V vs. Ag/AgCl. This was also recorded previously in ammonium bromide environments [11]. The sharp increase in the current densities is attributed to the following anodic reactions, related to the evolution of free  $\text{Br}_2$  or gaseous oxygen:



The formation of elemental bromine is clearly seen by the appearance of a red-brown color near the anodic surface. The free bromine appears at a potential near the redox potential - above 1 V vs. Ag/AgCl. Actually, when it reached the anodic surface, it became electrically conductive.

The exposure of Ti-2 to saturated NaBr solution, under high anodic potential, does not show positive hysteresis. The passive film obtained shows good electrical conductivity with no evidence to pitting formation. This finding was confirmed by SEM observations as presented in Fig. 2. These

images clearly show that increasing the concentration of bromide from 0.01 to 1 M leads to severe pitting attack; however, in the saturated solution pitting attack cannot be identified.

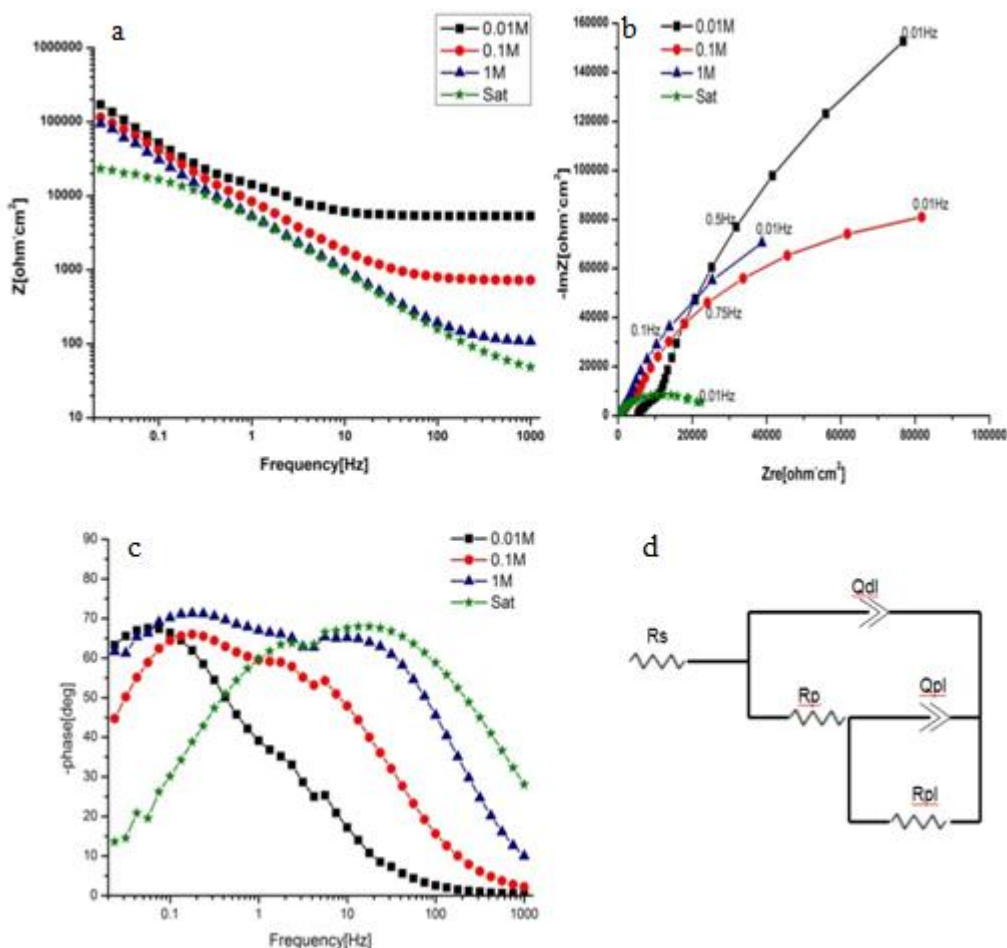


**Figure 3.** EIS spectra for passivity range of Ti-2 as a function of NaBr concentration: (a) Bode diagram (b), Nyquist diagram, (c) Bode phase diagram and (d) equivalent electrical circuit.

**Table 2.** Equivalent circuit parameters for titanium in NaBr solutions at passive range

NaBr[M]	$R_s$ ( $\Omega \cdot cm^2$ )	$Q_{dl}$ [F]	$\alpha_2$	$R_p$ ( $\Omega \cdot cm^2$ )	$Q_{pl}$ [F]	$\alpha_2$	$R_{pl}$ ( $\Omega \cdot cm^2$ )
0.01	5328.0	$59 \cdot 10^{-6}$	0.9	18477.0	$80.9 \cdot 10^{-6}$	0.9	707953.5
0.1	679.5	$0.15 \cdot 10^{-6}$	0.7	5375.5	$2.3 \cdot 10^{-6}$	0.9	604642.5
1	117.0	$62.6 \cdot 10^{-6}$	1	4059.0	$0.1 \cdot 10^{-6}$	1	122206.5
Sat	36.0	$0.2 \cdot 10^{-6}$	0.8	585.0	$53.8 \cdot 10^{-6}$	0.27	28431.0

The impedance spectra of Ti-2 in NaBr solutions were obtained over the passive anodic region (Fig. 3a-d), in all cases, it is possible to see two different time constant in the Nyquist diagrams, which are expressed by clearly two semi circles (Fig. 3b). The equivalent electrical circuit in Fig. 3d, which is composed of the passive layer dielectric material composed of  $TiO_2$  capacitance,  $Q_{pl}$ , combined in parallel with the double layer capacitance  $Q_{dl}$ ; the capacitances shown in this circuit are

mathematically modeled using a constant phase element (CPE) in order to consider the electrochemical behavior of system which do not correspond exactly to a pure capacitance. According to the Bode diagram (Fig. 3a), the total impedance decreases within the concentration from 720 kΩ in 0.01 M to 135 kΩ in 1 M and 32 kΩ in saturated NaBr solutions. These results indicate an increase with conductivity of the metal anodic surface with increasing bromide concentration. It might be related to bromide ions which act as electron donors to the TiO<sub>2</sub> passive layer. Table 2 summarizes all the parameters obtained from EC-Lab® V10.0 software after receiving the maximum match.

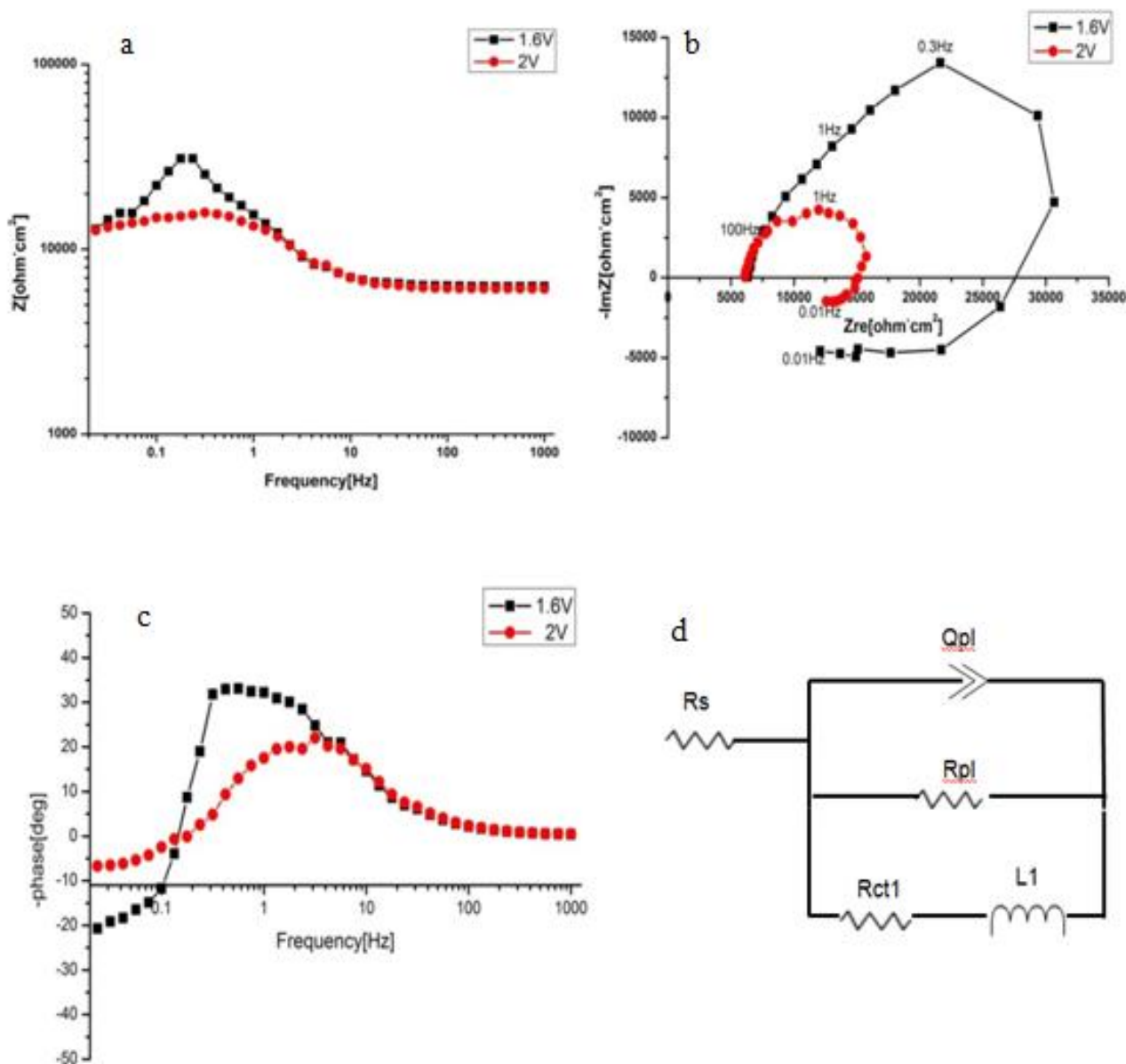


**Figure 4.** EIS spectra for Ti-2 in 0.01 M NaBr at the transpassive area: (a) Bode diagram (b) Nyquist diagram (c) Bode phase diagram and (d) equivalent electrical circuit.

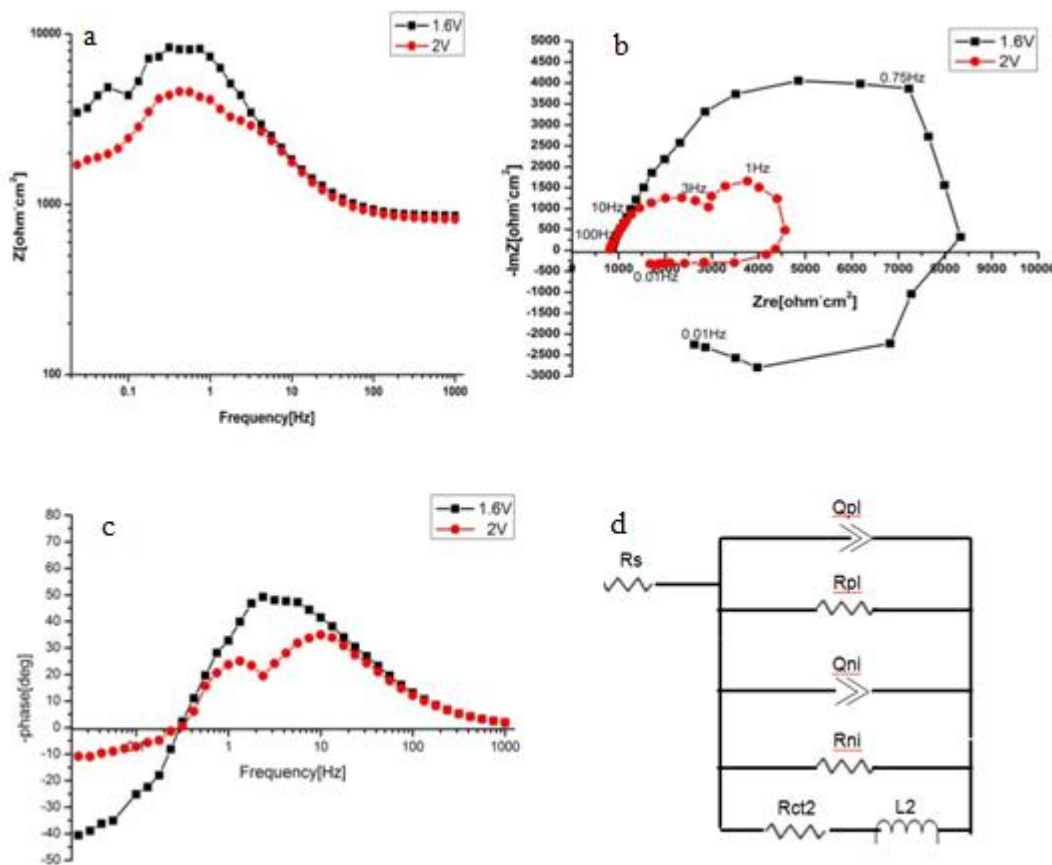


**Figure 5.** EIS spectra for Ti-2 in 0.1 M NaBr at the transpassive area: (a) Bode diagram, (b) Nyquist diagram, (c) Bode phase diagram and (d) equivalent electrical circuit

Figures 4-6 and Tables 3-5 reveal that each impedance diagram of the titanium electrode exposed to NaBr solutions up to 1 M is under 1.6 V vs. Ag/AgCl, consisting of a large capacitive loop at high frequencies (HF) and a small inductive one at low frequency (LF). The HF capacitive loop could be related to the passive layer and its dielectric properties and the LF inductive loop may be attributed to the initiation of the pitting process. The inductive coil represents the incubation stage during the anodic dissolution and propagation of the active pits formed on the anodic surface. The presence of this electrical element is expressed by a sharp decrease of the passive layer resistance, as present in the Bode diagram.

**Table 3.** Equivalent circuit parameter for titanium in 0.01M NaBr solutions under anodic potentials higher than the typical breakdown potential (under transpassivity)

[V] vs. Ag/AgCl	$R_s$ ( $\Omega \cdot cm^2$ )	$Q_{pl}$ [F]	$\alpha_1$	$R_{pl}$ ( $\Omega \cdot cm^2$ )	L [H]	$R_{ct}$ ( $\Omega \cdot cm^2$ )
1.6	6318.0	$78.9 \times 10^{-6}$	0.8	29322.0	11756.0	24511.5
2.0	6183.0	$53.1 \times 10^{-6}$	0.9	11686.5	3304.0	3051.0

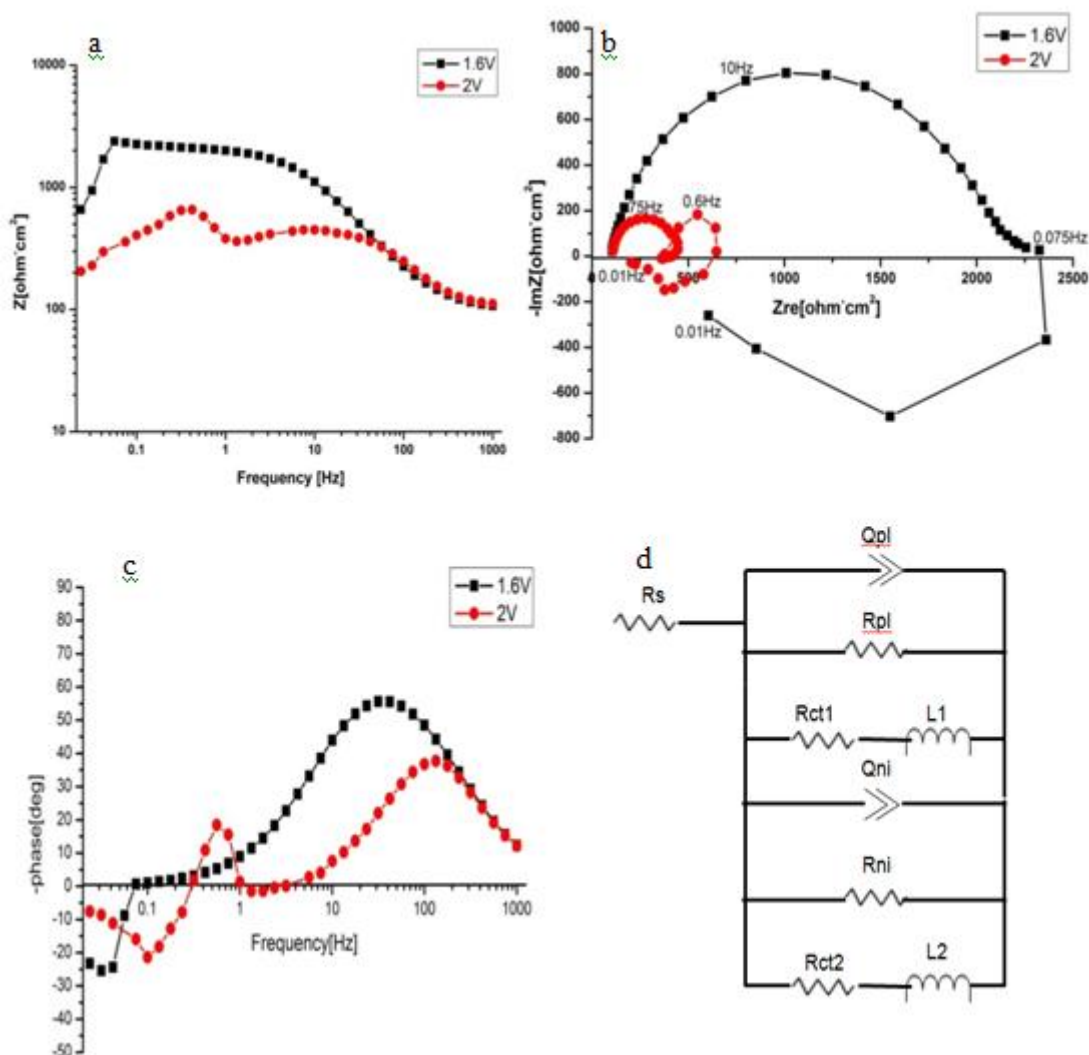


**Figure 6.** EIS spectra for Ti-2 in 1 M NaBr at the transpassive area: (a) Bode diagram, (b) Nyquist diagram, (c) Bode phase diagram and (d) equivalent electrical circuit

**Table 4.** Equivalent circuit parameter for titanium in 0. 1M NaBr solutions under anodic potentials higher than the typical breakdown potential (under transpassivity)

[V] vs Ag/AgCl	$R_s$ $\Omega \cdot cm^2$	$Q_{pl}$ [F]	$\alpha_1$	$R_{pl}$ $\Omega \cdot cm^2$	$Q_{ni}$ [F]	$\alpha_1$	$R_{ni}$ $\Omega \cdot cm^2$	L [H]	$R_{ct}$ $\Omega \cdot cm^2$
1.6V	860.8	$9.5 \times 10^{-6}$	0.8	9373.5	--	--	--	5418.0	1728.0
2.0V	487.4	$5.1 \times 10^{-6}$	0.2	4518.0	$0.1 \times 10^{-3}$	0.8	328.5	2772.0	2996.5

**Table 5.** Equivalent circuit parameter for titanium in 1 M NaBr solutions under anodic potentials higher than the typical breakdown potential (under transpassivity)

[V] vs Ag/AgCl	$R_s$ $\Omega \cdot cm^2$	$Q_{pl}$ [F]	$\alpha_1$	$R_{pl}$ $\Omega \cdot cm^2$	L1 [H]	$R_{ct1}$ $\Omega \cdot cm^2$	$Q_{ni}$ [F]	$\alpha_2$	$R_{ni}$ $\Omega \cdot cm^2$	L2 [H]	$R_{ct}$ $\Omega \cdot cm^2$
1.6V	99.0	$89.3 \times 10^{-6}$	0.9	1953.0	1741	877.5	--	--	--	--	--
2.0V	103.5	$46.6 \times 10^{-6}$	0.9	355.5	0.4	369.0	$8.0 \times 10^{-3}$	1	310.5	87.0	234.0

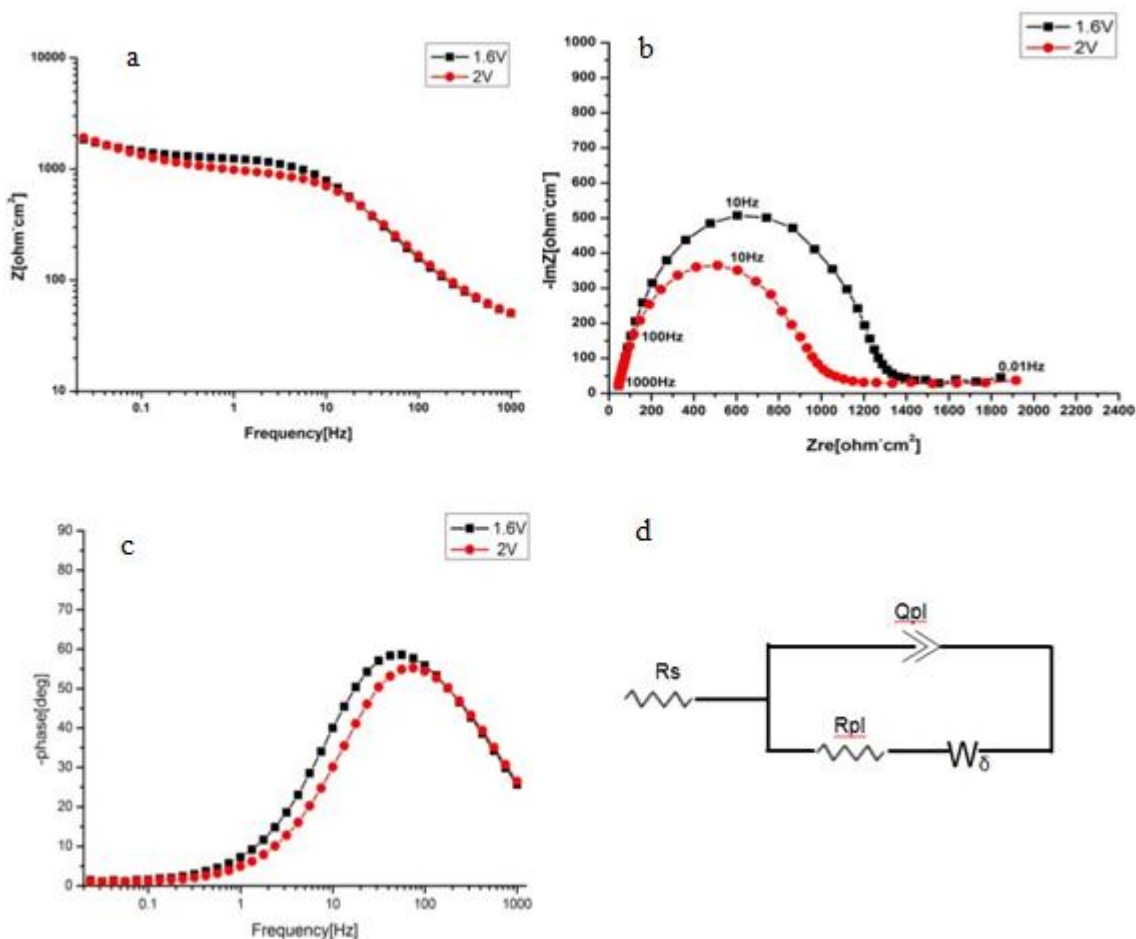


**Figure 7.** EIS spectra for Ti-2 in saturated NaBr at the transpassive area: (a) Bode diagram, (b) Nyquist diagram, (c) Bode phase diagram and (d) equivalent electrical circuit.

**Table 6.** Equivalent circuit parameter for titanium in saturated NaBr solutions under anodic potentials higher than the typical breakdown potential (under transpassivity)

[V] vs Ag/AgCl	$R_s$ ( $\Omega \cdot cm^2$ )	$Q_{pl}$ [F]	$\alpha_1$	$R_{pl}$ ( $\Omega \cdot cm^2$ )	$R_d$ ( $\Omega \cdot cm^2$ )	$t$ (s)
1.6	58.5	$60.8 \times 10^{-6}$	1	1080.0	1069.6	31
2.0	54.0	$54.1 \times 10^{-6}$	1	976.5	702.0	69

In several occasions, the ending stage of the primary pit propagation were recognized when the pits have become inactive, as presented for 0.1 M NaBr in 2 V vs. Ag/AgCl (Fig. 5b). The primary pits were the first points where the passive film started to breakdown and the anodic dissolution process had continued on these sites. In the next step, a second capacitor has been developed on the passive surface obtained on the new surface created by the anodic dissolution. The secondary pits developed on this dielectric layers were represented by the inductive semi-circle. In 1 M NaBr in 2 V the EIS had indicated primary and secondary pits formation, as presented in Fig. 6. The primary pits formation is demonstrated as an active coil within the intermediate frequencies, while the secondary ones, as an active coil within the lower frequencies connected to the second semicircle. Moreover, submission of a

higher anodic potential causes the inductive coil to appear at even lower frequencies in the Nyquist diagram. This shift to lower frequencies indicates a longer period for relaxation, meaning a longer duration of activity for each active pit, enhancing a severe attack. In this case, the electrical equivalent circuit shows two inductive coils and two capacitors, which act in parallel, analogous to two different types of active pits that act in parallel on different locations on the anodic surface (Fig. 6d).

Examining the electrochemical behavior of titanium exposed to a saturated NaBr solution, may not lead to the presence of inductive coil, even when increasing the anodic potential above the typical breakdown potential (Fig. 7a-d). Nyquist diagrams show a clear semi-circle at high frequencies and a resistance time dependent (Rtd) at low frequency values. Unlike resistors mentioned above, this electric element is time-dependent, meaning a resistor that presents development of resistivity within time. The Bode diagrams show an increase in the ohmic resistance within the range of the lower frequencies. These findings obtained only under saturation; indicate that, in contrary to expectations, breakdown of the passive layer did not occur on the anodic surface, even under potentials higher than breakdown. Furthermore, under saturated conditions increasing the potential up to 2 V resulted with higher ohmic resistance, indicating a thicker passive film. According to [19-21], the Rtd electrical element indicates a diffusion control process that may be related to the solid state diffusion process, taking place during the passive film development when applying the anodic potential.

The XPS experiments were performed in order to estimate the thickness of titanium oxides that was formed on the sample during the exposure to 2 V potential over the mentioned NaBr solutions. According to the results, the ratio between the titanium and oxygen atomic percent is 1:2, respectively. The increase of the bromide concentration up to 1 M leads to decrease of the passive layer thickness from 10 to 6 nm, as presented in Fig. 8 a,b. However, under saturation conditions an increase in titanium oxide film thickness can be observed, approximately 11 nm (Fig. 8c). This finding is consistent with the results of the electrochemical experiments described above. As mentioned, the Rtd element appears only under saturation and pointed on increase of the ohmic resistance at lower frequencies scanning. XPS analysis clearly shows that under saturation the passive TiO<sub>2</sub> film became much thicker. This is coherent with the EIS findings and it means that the surface of the metal became more immune to the chemical environment, even if it looks more active. This anomalous behavior under saturation matches the observations in ammonium bromide solutions [11].

This anomalous pitting behavior under saturation may be attributed to a change in the molecular structure of water. In attempt to get some insight regarding this effect and to propose a mechanism to understand this phenomenon, Raman spectroscopy has been used. This is since it is anticipated that as the salt is dissolved in aqueous NaBr solutions, the water molecules form hydration shells around the dissolved ions that perturb the hydrogen bond network. Therefore, the surrounding hydrogen bonds alter the intermolecular bonding and are expected to change the vibrational spectra, implying that Raman spectroscopy of the O-H stretching region can be applied to investigate the hydrogen bonding in water.

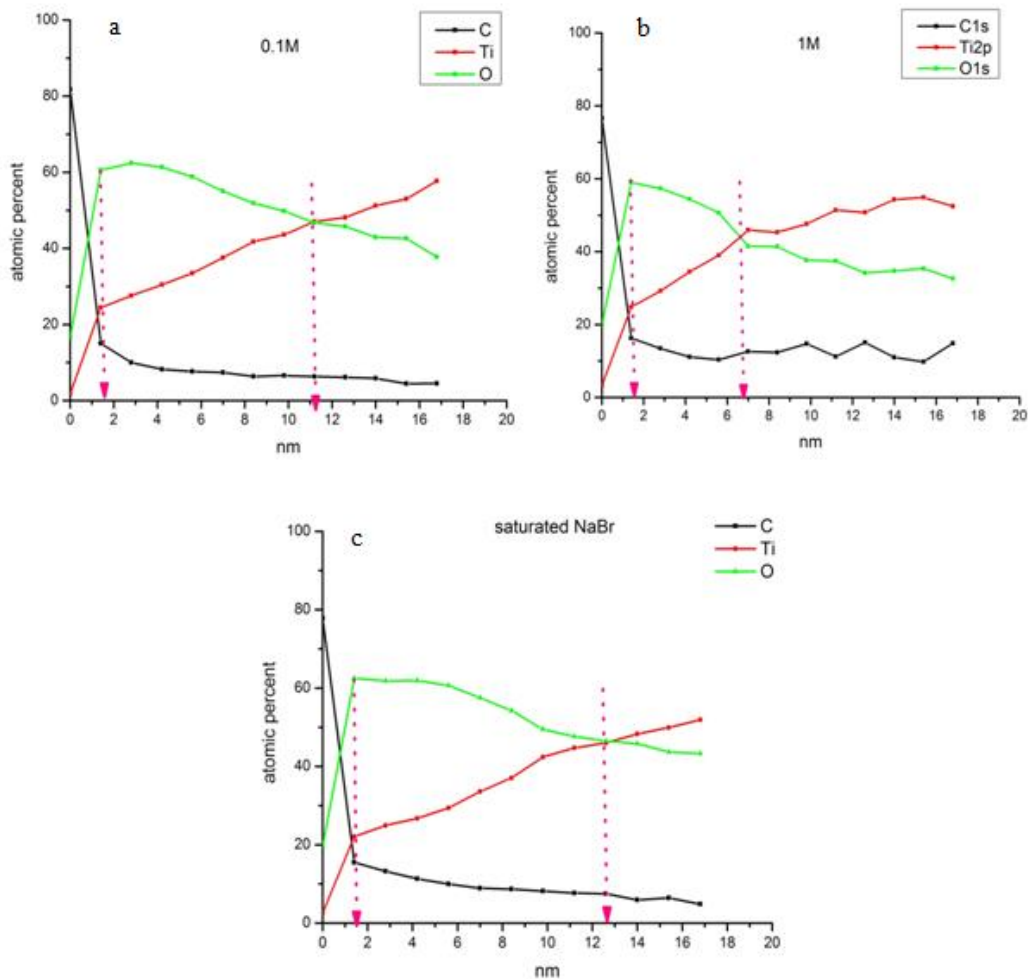


**Figure 8.** XPS analysis for Ti-2 after exposure to potential in transpassive area: (a) 0.1 M, (b) 1 M and (c) saturated NaBr.

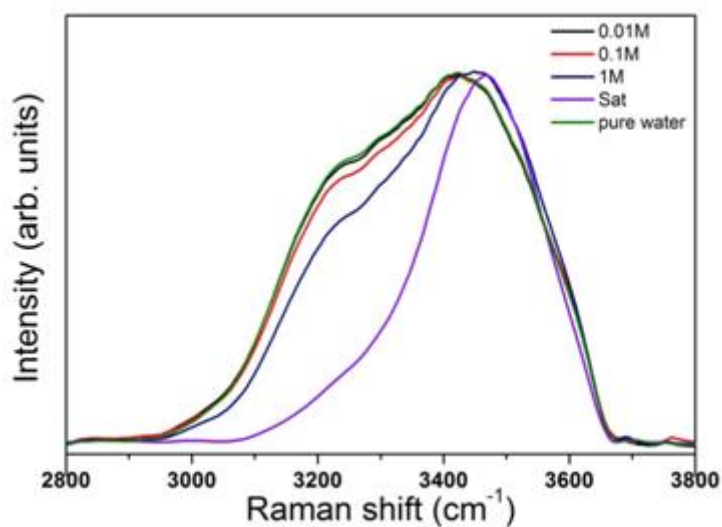


**Figure 9.** Raman spectra of pure water as well as of NaBr solutions of different concentrations, up to saturation in the O-H stretching region (2800 - 3800 cm<sup>-1</sup>).

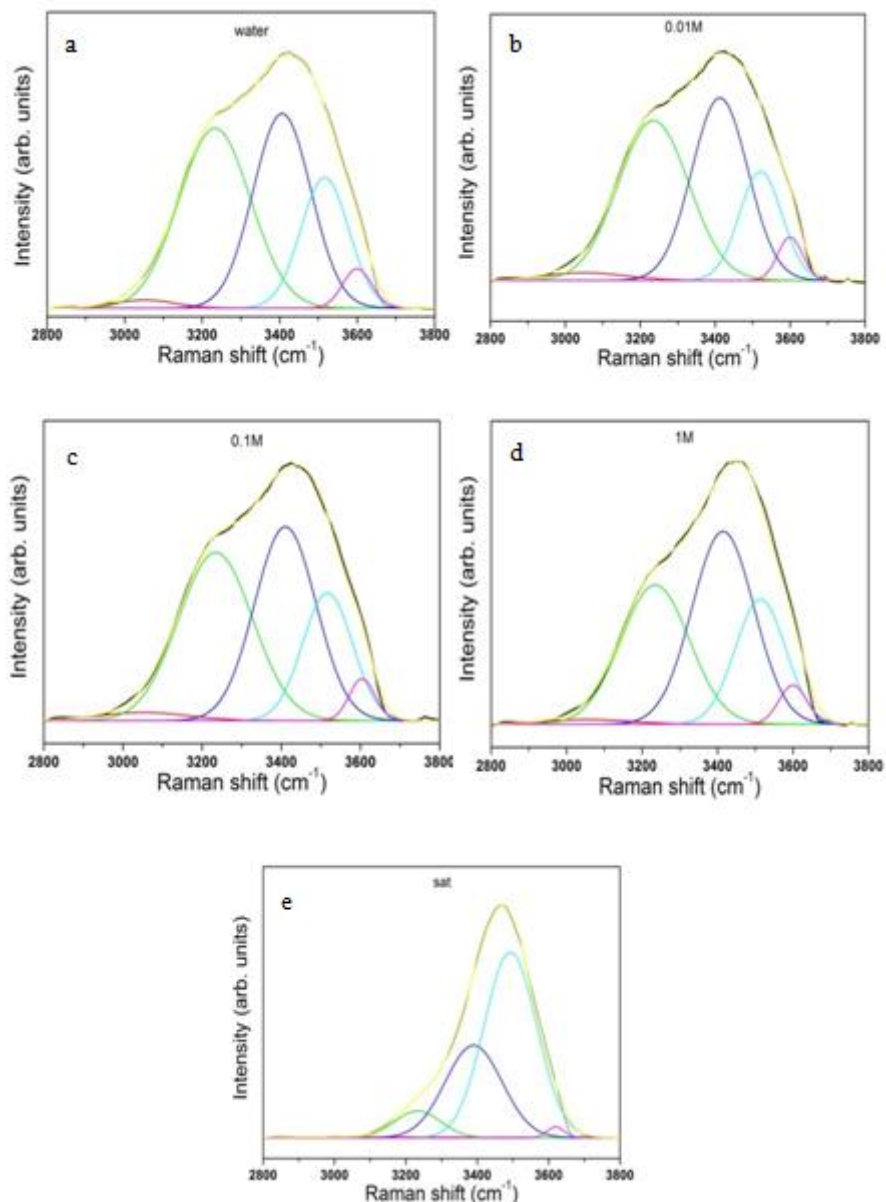


**Figure 10.** Deconvolution of the Raman spectra of pure water at 298K and of the different solutions, when they are fitted by five Gaussians

Figure 9 shows the Raman spectra of pure water as well as of NaBr solutions of different concentrations, up to saturation in the O-H stretching region (2800 - 3800  $\text{cm}^{-1}$ ). All the spectra were normalized to the maximum peak height for comparison. It is clearly seen that very broad features appear in each spectrum, with very different widths and with some shoulders that lead to distinctive shapes for different concentrations. Since the contour of the Raman O-H stretching band is so complex and broad, it is difficult to directly obtain information on the water structure from it. Therefore, Gaussian analysis was used to investigate the O-H stretching bands in the different solutions. Figure 10a-d shows the deconvolution of the Raman spectra of pure water at 298 K and of the different solutions, when they are fitted by five Gaussians ref. It is clearly seen that the observed bands are well fitted by the five Gaussians, although their intensity ratios are changed for the different solutions.

As mentioned, each Gaussian element indicates a particular configuration of the water structure. Generally, the 3051 and 3233  $\text{cm}^{-1}$  components are assigned to fully hydrogen bonded water molecules, while those of 3393 and 3511  $\text{cm}^{-1}$  to partly hydrogen bonded water molecules and the 3628  $\text{cm}^{-1}$  component refers to free water molecules, i.e., without hydrogen bonds [22]. According to Figs. 10a -10d, the intensity of the 3233  $\text{cm}^{-1}$  component decreases with increasing bromide concentration; it means that the tetrahedral structure of water has broken. In fact, once reaching the saturated solution, the intensity of the 3233  $\text{cm}^{-1}$  component completely fades away. In addition, the highest peak at 3511  $\text{cm}^{-1}$  indicates a shift to high wavenumber under saturation conditions. This may result in the formation of halogen ion-water hydrogen bond. In diluted solutions this shift is considered negligible. The main change which cannot be neglected is the decrease of the component 3628  $\text{cm}^{-1}$  under saturation condition. This character presents the quantity of free water molecules. Suppression of this peak, when the content of NaBr becomes saturated, indicates reduction in free water molecules. This may contribute to the explanation of the anomalous behavior under saturation: pitting mechanism is sharply disturbed; therefore, incubation and propagation of active pits on the titanium are inhibited under saturation conditions.

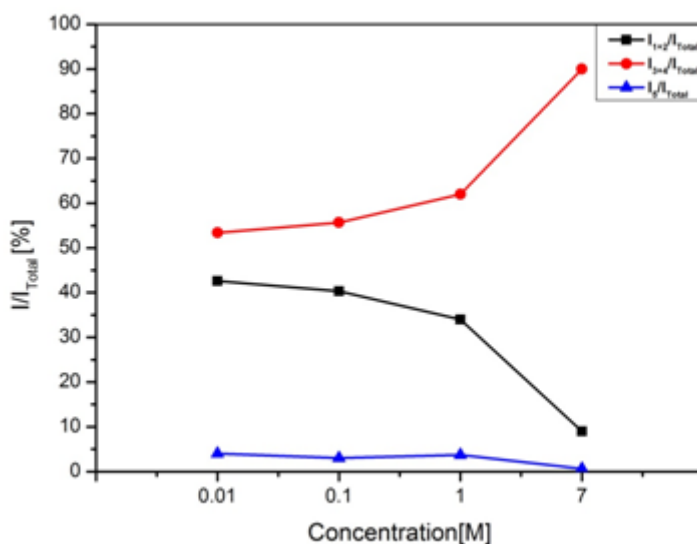


**Figure 11.** The relative area of particular peaks in ratio to the total area of the spectrum as a function of the halogen concentration.

To evaluate the changes taking place in the water molecules as a function of the halogen concentration, the ratio between the relative area of the corresponding peaks under the curve to the total area of the spectrum was determined (Fig 11). In Fig. 11 the ratio of sum of areas of the first and second peaks to the total area as a function of concentrations was calculated. As mentioned, these two peaks are attributed to breaking of hydrogen bonds. It is clearly seen that increase in bromide concentration leads to the decrease in the relative area, meaning presence of less water molecules with full hydrogen bonds. The most significant change is observed for the saturated solution. Figure 11

presents the ratios for the sum of the areas of peaks 3 and 4 which are typical to the bond between hydrogen and water molecules. As previously discussed, the change is negligible within the bromides concentration increase up to 1M, unlike in saturated solution where these peaks are being a significant part of the total area spectrum. That is the reason for noting, that despite of the maximal break of the tetrahedral structure of water molecules, they have a tendency to compensate by halogen-water bonds creation. Meaning, by getting near saturation conditions there is an equal competition between the electrostatic forces and the neighbors water intermolecular forces, giving compensation and balance. This assumption is verified by analyzing Gaussian peak 5, appearing at  $3628\text{ cm}^{-1}$ . One can conclude that in the presence of a saturated solution there is a decrease in the content of free water molecules, meaning, that despite the full hydrogen bonds of water, halogen-water bonds are formed compensating the breaking. Therefore, altogether the amount of free water molecules becomes negligible.

In the diluted solutions the observed change in the Raman spectra was the decrease in the intensity of the first two peaks, which indicates the hydrogen bonds breaking. Hence, for diluted solutions, one can assume with a high probability that the free bromide ions concentration is the dominant parameter, which provides enhanced sensitivity to local corrosion. Thus, the leading conditions for pitting corrosion development in diluted solutions are external voltage above the pitting potential and critical concentrations of halides which are absorbed on the metal surface.

#### 4. CONCLUSIONS

- Anomalous behavior of Ti-2 in saturated NaBr solution was detected. Under saturation conditions pitting was not observed, even when the anodic electrical field was above breakdown.
- In NaBr diluted aqueous solutions pitting sensitivity was detected and EIS indicated the formation of anodically active pits by the appearance of inductive loops.
- XPS analysis clearly showed that under saturation the passive film,  $\text{TiO}_2$ , became much thicker.
- Raman spectroscopy had confirmed that the amount of free water molecules is negligible under saturation conditions and in fact the ultimate majority of water molecules are bounded to the dissolved ions. In diluted solution, no significant changes were observed in the Raman spectra. It is thus clearly shown that the leading conditions for pitting corrosion development in diluted solution are external voltage above the pitting potential and the critical concentrations of halides which are absorbed on the metal surface.

#### References

1. K.Wang, *Mater. Sci. Eng. A*, 213 (1996) 134-137.
2. J. Pan, D. Thierry and C. Leygraf, *Electrochim. Acta* 41( 1996) 1143-1 153.
3. Sergio Luiz de Assis, Stephan Wolynech, Isolda Costa, *Electrochim. Acta* 51 (2006) 1815-1819/
4. D. Itzhak, T. Greenberg, *Mater. Sci. Eng. A*. 302 (2001) 135-140.
5. F. El-Taib Heakal, Kh.A. Awad, *Int. J. Electrochem. Sci.* 6 (2011) 6483-6502.
6. J.L. Trompette, L. Massot, L. Arurault and S. Fontorbes, *Corros. Sci.* 53 (2011) 1262-1268.

7. I. Dugdale and J. B. Cotton, *Corros. Sci.* 4 (1964) 397-411.
8. S. Huo and X. Meng, *Corros. Sci.* 31(1990) 281-286.
9. T.R. Beck, *J. Electrochem. Soc.* 120 (1973) 1310-1316.
10. E. Blasco-Tamarit, A. Igual-Mun˜oz, J. Garcı́a Anto´n, D. Garcı́a-Garci´a, *Corros. Sci.* 49 (2007) 1000–1026.
11. R. Ittah, E. Amsellem and D. Itzhak, *Int. J. Electrochem. Sci.* 9 (2014) 633-643.
12. O.Y. Samoilov, In water and aqueous Solution; Structure, Thermodynamic and Transport Processes; Wiley-Interscience; New York , 1972; pp 597-612.
13. O.Y. Samoilov, *Discuss. Faraday Soc.* 24 (1957) 141-146.
14. B. Hribar et al. *J. Am. Chem. Soc.* 124 (2002) 12302-12311.
15. <http://www.sas.upenn.edu/~crulli/RamanBasics.html>
16. R.Li, Z. Jiang, F. Chen, H. Yang and Y. Guan, *J. Mol. Structure* 707 (2004) 83-88.
17. E. Kikuti, R. Conrado, N. Bocchi, S.R. Biaggio and R. C. Rocha-Filho, *J. Braz. Chem. Soc.* 15 (2004) 472-480.
18. L. Tan, R.A. Dodd, and W.C. Crone. *Biomaterials*, 24 (2003) 3931-3939.
19. H. Sakly, R. Mlika, I. Bonnamour, F. Aouni, H. Ben Ouada and N. Jaffrezic Renault, *Electrochim. Acta* 52(2007) 3697-3703.
20. M.C. Lefebvre, B.E. Conway, *J. Electroanal. Chem.* 480 (2000) 34–45.
21. V. F. Lvovich and M. F. Smiechowski, *Electrochim. Acta* 51 (2006) 1487–1496.
22. D.M. Carey and G.M. Korenowski, *J. Chem. Phys.* 108 (1998) 2669-2675.

© 2015 The Authors. Published by ESG ([www.electrochemsci.org](http://www.electrochemsci.org)). This article is an open access article distributed under the terms and conditions of the Creative Commons Attribution license (<http://creativecommons.org/licenses/by/4.0/>).